Electronic Supplementary Information for

Influence of isovalent 'W' substitutions on the structure and electrical properties of $La_2Mo_2O_9$ electrolyte for intermediate-temperature solid oxide fuel cells

Tanmoy Paul*,† and Yoed Tsur

Department of Chemical Engineering and the Grand Technion Energy Program, Technion-Israel Institute of Technology, Haifa 3200003, Israel;

(Y.T.) tsur@technion.ac.il

* Correspondence: paultanmoy00@gmail.com

† Present address: Department of Condensed Matter Physics and Materials Science, S. N. Bose National Centre for Basic Sciences, Kolkata 700098, India

Table S1. The room temperature X-ray diffraction Rietveld refinement agreement factors for different samples.

Here, R_{exp} is a statistical evaluation of the noise in the XRD data and R_{wp} is defined as a weighting function to place more emphasis on good fit between high intensity data points and less emphasis on low intensity data points and Goodness of Fit is defined as $\chi^2 = {R_{wp}^2}/{R_{exp}^2}$. The unit cell parameters and cell volume are also shown.

Composition (x)	Lattice parameters (Å)	Volume (Å³)	R_{wp}	R_{exp}	χ^2
0-Cubic	7.1490	365.372	0.319	0.0740	18.57
0-Monoclinic	a = 14.3293 b = 21.4825 c = 28.5864 β = 90.4104°	8799.554	0.055	0.048	1.31
0.5	7.1542	366.173	0.418	0.214	3.821
1.0	7.1472	365.105	0.222	0.12	3.420
1.25	7.1501	365.542	0.264	0.198	1.769
1.5	7.1436	364.546	0.244	0.124	3.875

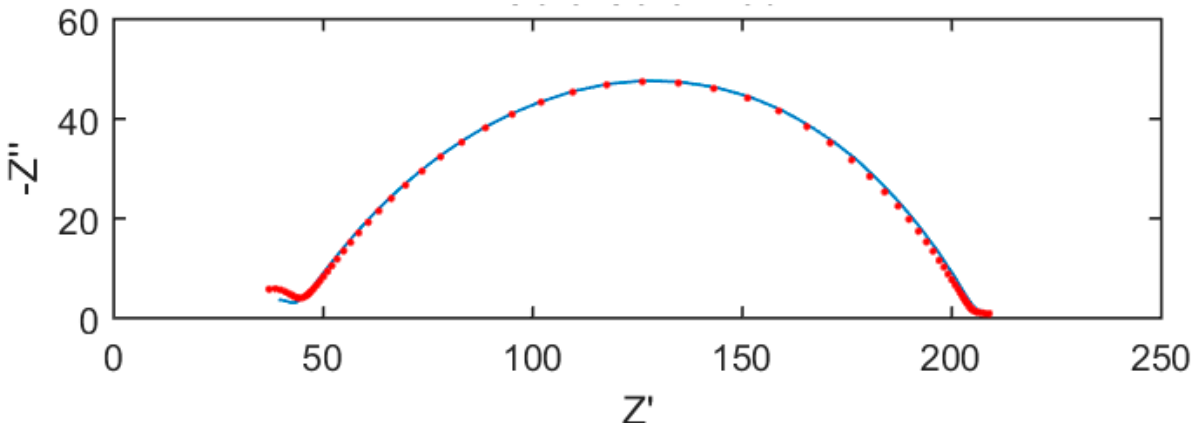

Figure S1. Typical validation of the Kramers Krönig relation is shown for 0.5W at 600°C. The solid line represents the data obtained by KK relation.

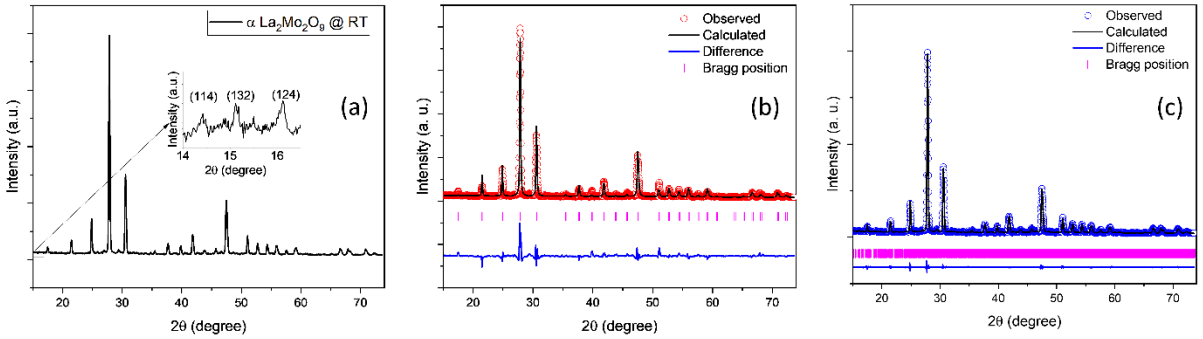

Figure S2. (a) Room temperature XRD pattern of α-$La_2Mo_2O_9$. Three Bragg peaks as detected from slow scan is shown in the inset. (b) and (c) are Rietveld refinement patterns of $La_2Mo_2O_9$ considering the cubic and monoclinic phase respectively. The refinement agreement factors in Table S1, suggest that room temperature pattern of $La_2Mo_2O_9$ is monoclinic (α phase).

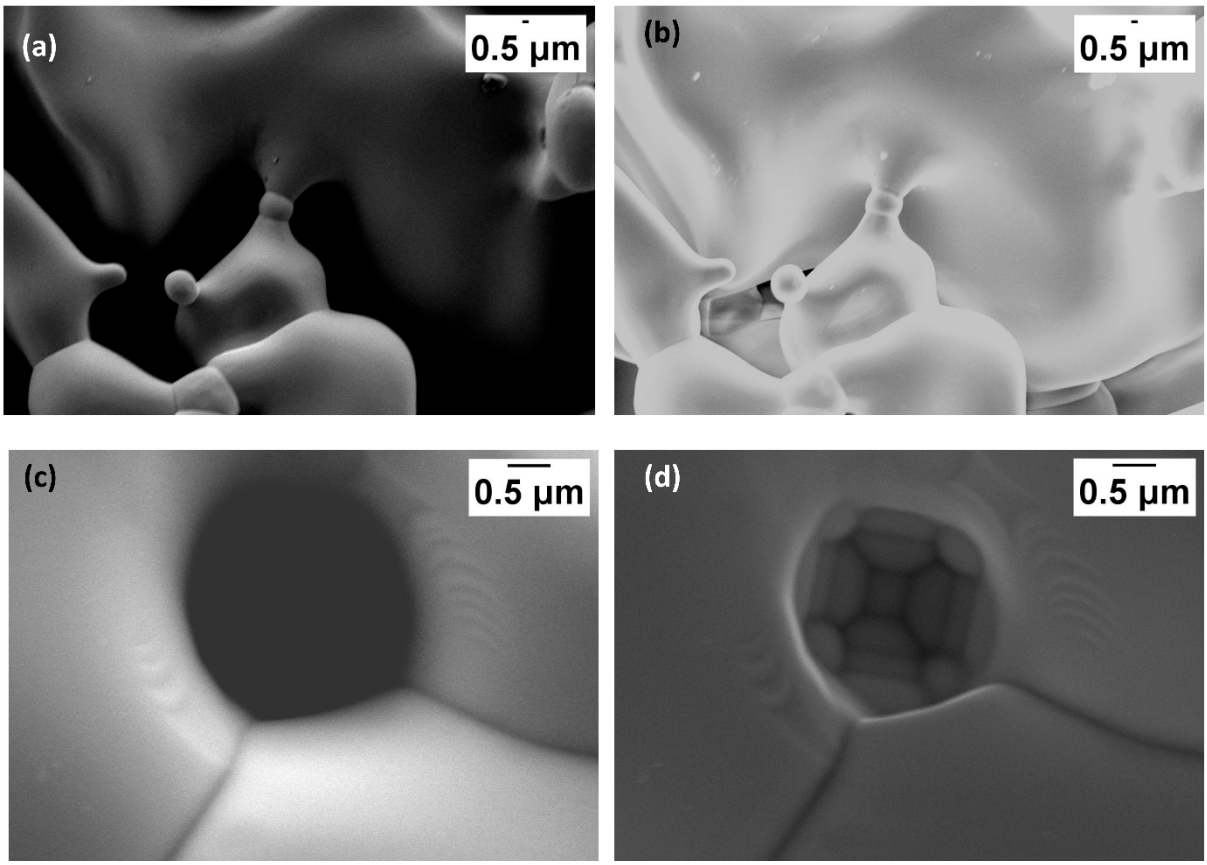

Figure S3. The depth of the pores is shown in SEM micrographs of (a) and (b) for 1.25W and (c) and (d) for 1.5W. In (a) and (b) the image contrasts are shown by changing secondary to in lens detectors respectively. The same experiment is also performed in (c) and (d) to identify the 'real' porosity of the samples.

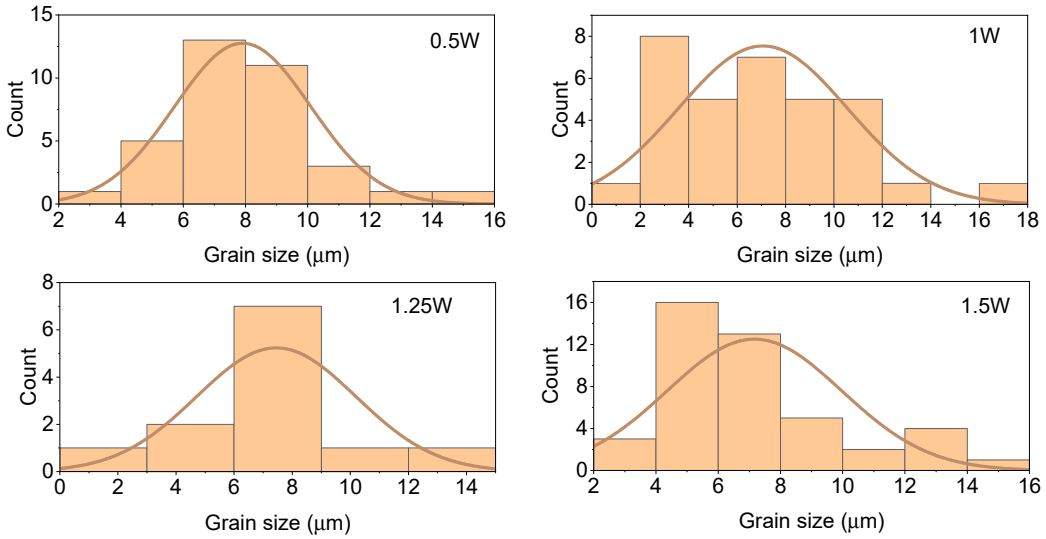

Figure S4. Histograms for evaluating the average grain size and the distribution of grain size for 0.5W, 1.0W, 1.25W and 1.5W.

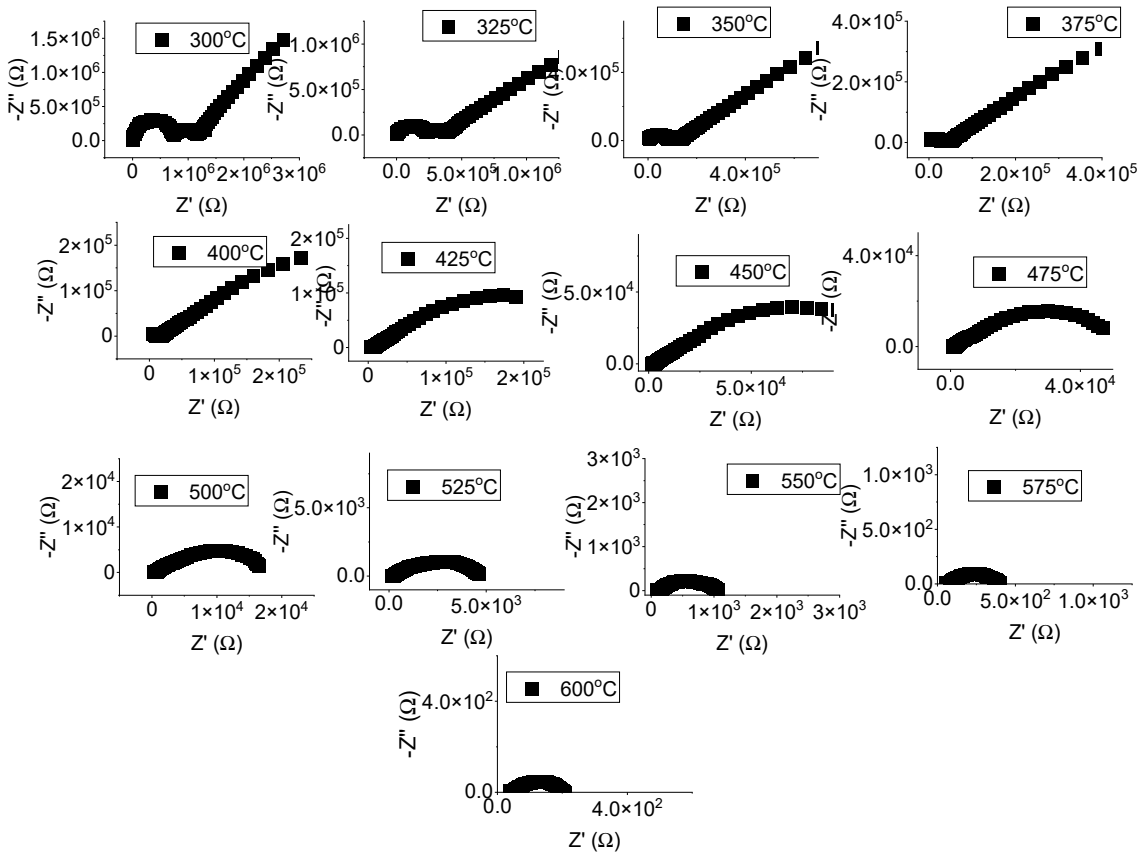

Figure S5. Nyquist plot of impedances at different temperatures for 0.5W.

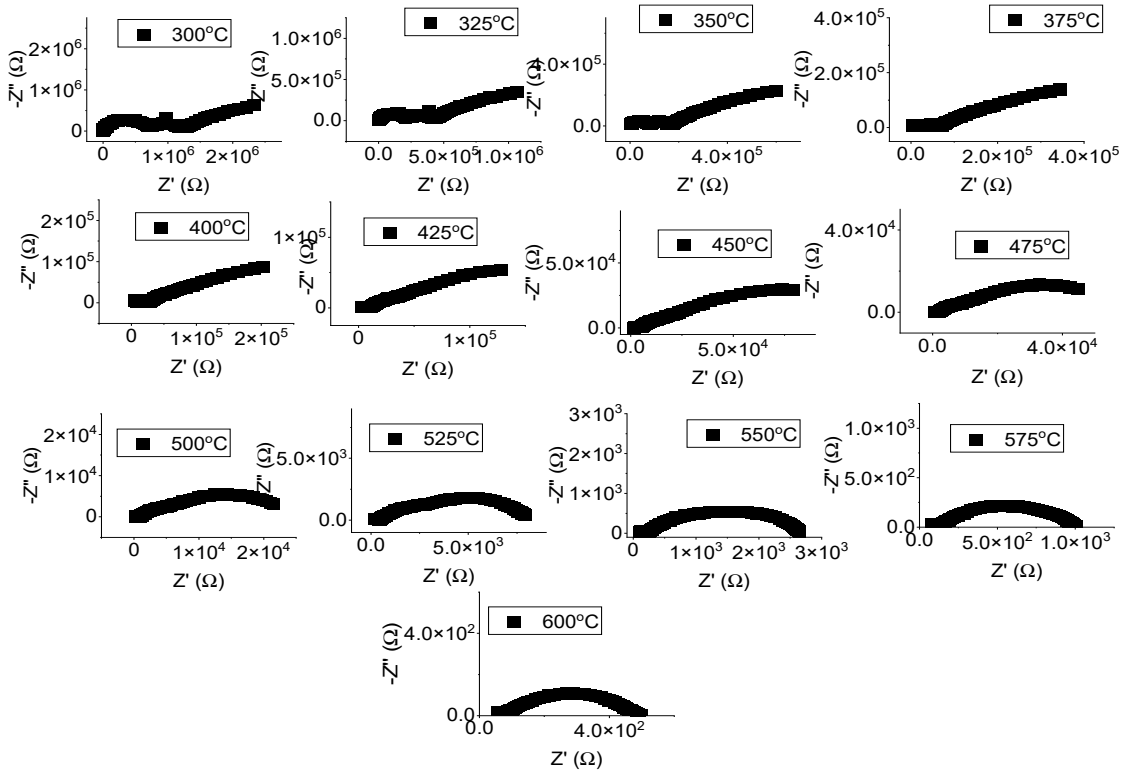

Figure S6. Nyquist plot of impedances at different temperatures for 1.0W.

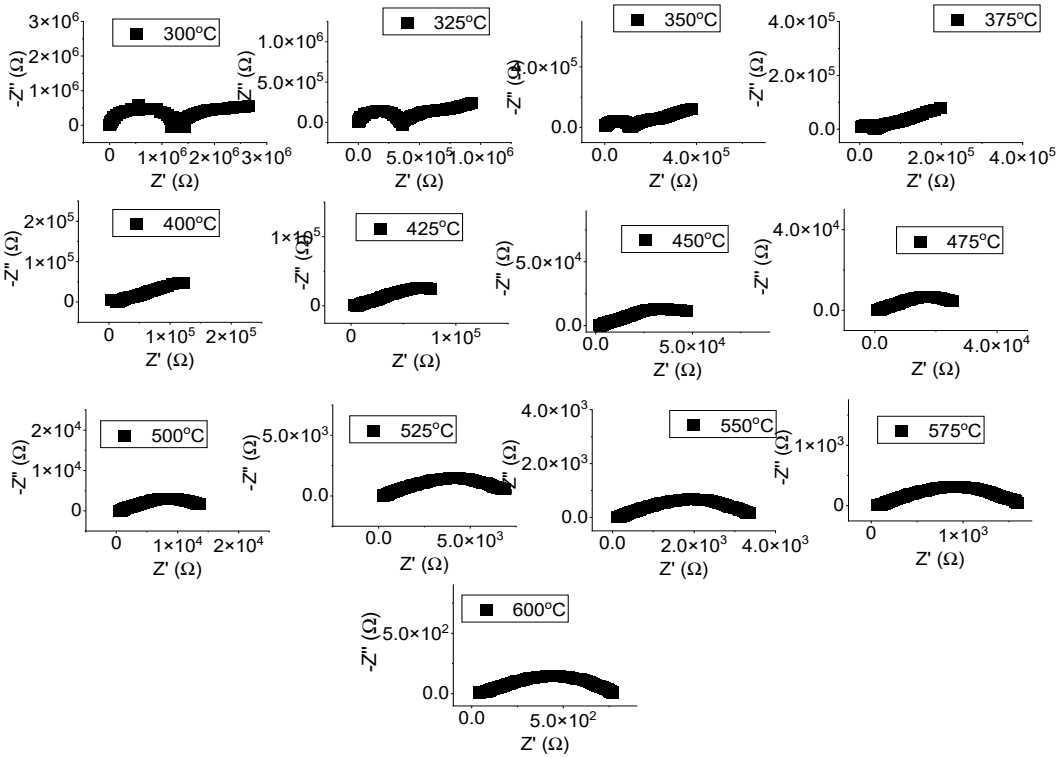

Figure S7. Nyquist plot of impedances at different temperatures for 1.25W.

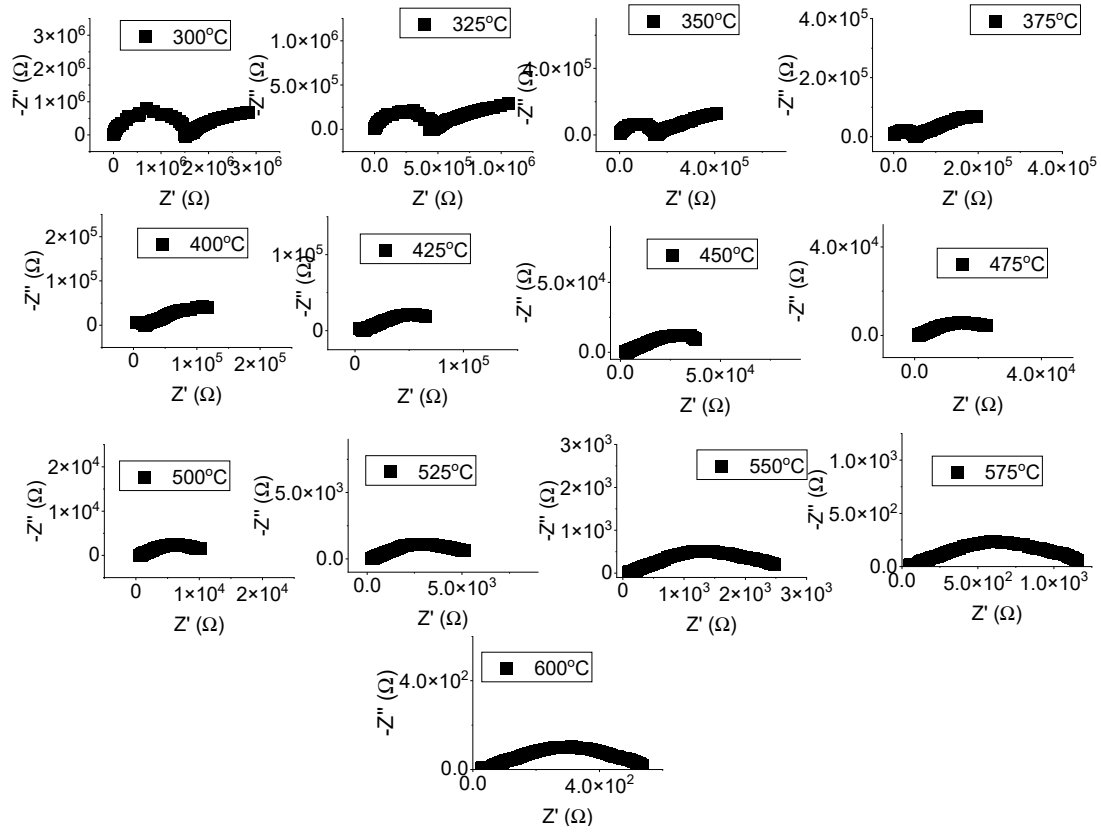

Figure S8. Nyquist plot of impedances at different temperatures for 1.5W.

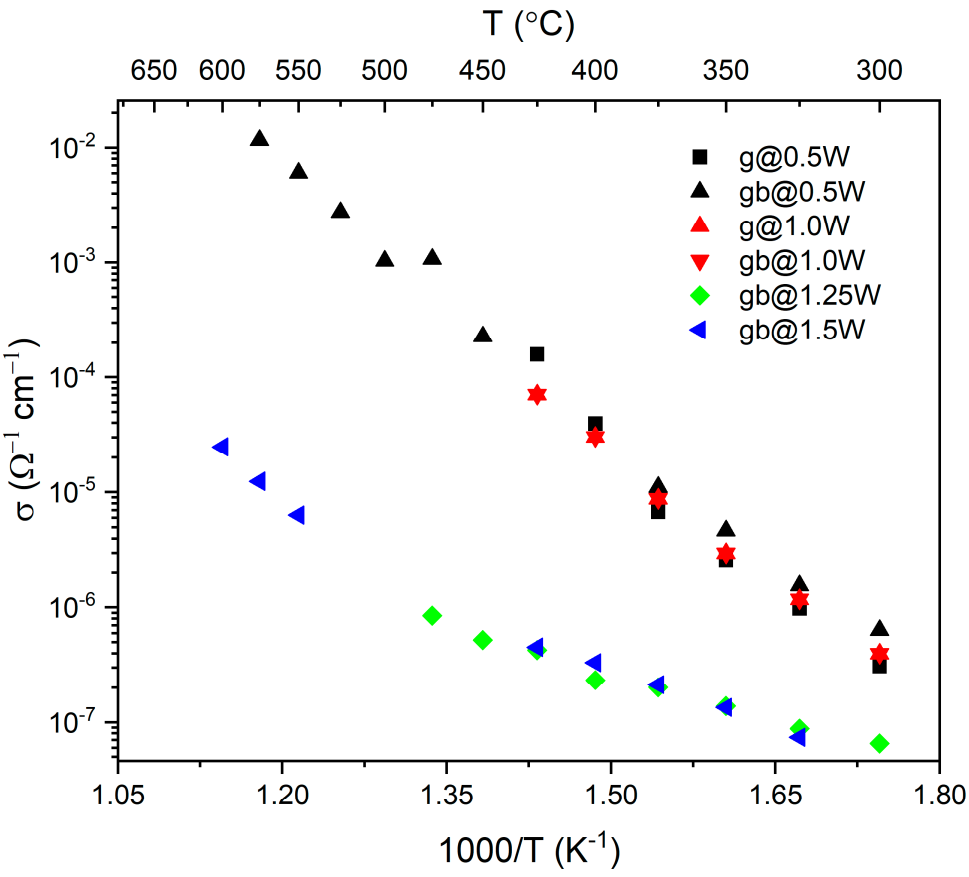

Figure S9. Reciprocal temperature dependence of grain and grain boundary conductivities. 'g': grain and 'gb': grain boundary. The linear least square fits are not shown for better clarity.